Molecular Dynamics Study of the 13-*cis* form (bR$_{548}$) of Bacteriorhodopsin and Its Photocycle

Ilya Logunov, William Humphrey, Klaus Schulten, and Mordechai Sheves
Beckman Institute and Departments of Chemistry, Physics, and Biophysics, University of Illinois at Urbana-Champaign, Urbana, Illinois 61801 USA

ABSTRACT   The structure and the photocycle of bacteriorhodopsin (bR) containing 13-*cis*,15-*syn* retinal, so-called bR$_{548}$, has been studied by means of molecular dynamics simulations performed on the complete protein. The simulated structure of bR$_{548}$ was obtained through isomerization of in situ retinal around both its C$_{13}$-C$_{14}$ and its C$_{15}$-N bond starting from the simulated structure of bR$_{568}$ described previously, containing all-*trans*,15-*anti* retinal. After a 50-ps equilibration, the resulting structure of bR$_{548}$ was examined by replacing retinal by analogues with modified β-ionone rings and comparing with respective observations. The photocycle of bR$_{548}$ was simulated by inducing a rapid 13-*cis*,15-*anti* → all-*trans*,15-*syn* isomerization through a 1-ps application of a potential that destabilizes the 13-*cis* isomer. The simulation resulted in structures consistent with the J, K, and L intermediates observed in the photocycle of bR$_{548}$. The results offer an explanation of why an unprotonated retinal Schiff base intermediate, i.e., an M state, is not formed in the bR$_{548}$ photocycle. The Schiff base nitrogen after photoisomerization of bR$_{548}$ points to the intracellular rather than to the extracellular site. The simulations suggest also that leakage from the bR$_{548}$ to the bR$_{568}$ cycle arises due to an initial 13-*cis*,15-*anti* → all-*trans*,15-*anti* photoisomerization.

INTRODUCTION

Bacteriorhodopsin (bR) is a protein composed of seven α-helices that spans the purple membrane of *Halobacterium halobium* and that functions as a light-driven proton pump. It is a member of the retinal protein family, which encompasses proteins with a retinal chromophore bound within the protein interior via a protonated Schiff base linkage to a lysine side chain. The retinal isomer composition in bR is 0.66 13-*cis* and 0.34 all-*trans* in the dark-adapted form of the pigment (DA), a ratio that is altered in mutants of bR$_{548}$ and in bacterial rhodopsins of other species. The two isomers denoted bR$_{548}$ (13-*cis*) and bR$_{568}$ (all-*trans*) absorb at 548 and 568 nm, respectively. Retinal in the bR$_{568}$ pigment exists in the all-*trans*,15-*anti* configuration, and in the bR$_{548}$ pigment in the 13-*cis*,15-*syn* configuration as suggested first in Orlandi and Schulten (1979) and observed in Harbison et al. (1984), Smith et al. (1984), and Livnah and Sheves (1993). Both the bR$_{568}$ and the bR$_{548}$ isomers undergo a characteristic photocycle (see Fig. 1) initialized in both cases by a photoisomerization involving rotation around the C$_{13}$-C$_{14}$ double bond. However, proton pumping is restricted to the photocycle of bR$_{568}$. The photocycle of bR$_{548}$ does not involve a vectorial proton translocation. The photocycle of native bR$_{548}$ leaks into the bR$_{568}$ form whereas the bR$_{568}$ photocycle replenishes only the bR$_{568}$ form. As a result, under the influence of light, any mixture of bR$_{568}$/bR$_{548}$ adopts to the bR$_{568}$ pigment, which is accordingly called the light-adapted form (LA). For recent reviews, see Khorana (1988), Birge (1990), Mathies et al. (1991), Lanyi (1992), Oesterhelt et al. (1992), and Ebrey (1993).

Three main questions arise concerning bR$_{548}$ and its photocycle. What factors determine the ratio of the bR$_{568}$ and the bR$_{548}$ forms? Why does the photocycle of bR$_{548}$ not pump protons and what does this fact tell us about the mechanism of proton pumping in bacteriorhodopsin? By what pathway is 15-*syn* retinal of bR$_{548}$ transformed to 15-*anti* retinal of bR$_{568}$ during light adaptation? The availability of the structure of bacteriorhodopsin (bR$_{568}$) reported by Henderson et al. (1990) provides an opportunity to answer these questions. A promising approach is provided by molecular dynamics simulations based on this structure.

Unfortunately, the structure in Henderson et al. (1990) is of relatively low resolution (e.g., water bound in the protein is not resolved) and also does not entail the interhelical loops. As a result, the loops needed to be added, the structure refined, and water added before molecular dynamics simulations could be carried out. In this paper, we extend previous molecular dynamics simulations (Nonella et al., 1991; Zhou et al., 1993; Humphrey et al., 1994) that focused on bR$_{568}$ to study the bR$_{548}$ pigment and its photocycle. As a test of the proposed bR$_{548}$ structure obtained, we examine the replacement of retinal by various analogues as well as investigate the properties of the D85A mutant of bR$_{548}$. The results of our simulations are compared with the relevant experimental observations (Rath et al., 1993; Ottolenghi and Sheves; 1989, Steinberg et al., 1991).

MATERIALS AND METHODS

The original structure of bR, as determined by Henderson et al. (1990) with electron microscopy, resolved the membrane-spanning helical residues; the interhelix loops had been added to this structure and equilibrated by molecular dynamics simulations in Nonella et al. (1991). The backbone atoms
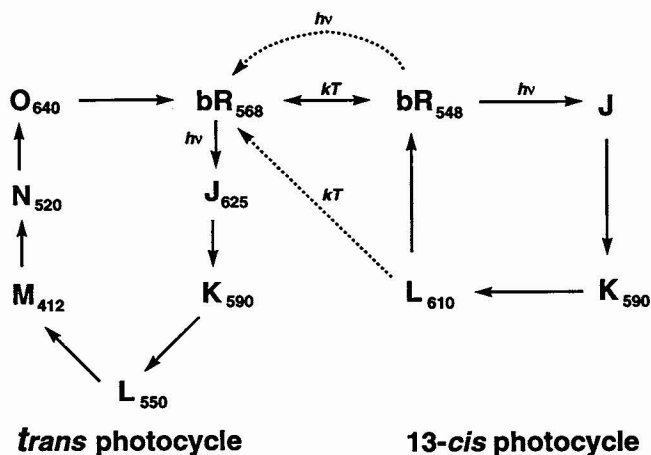
FIGURE 1 Photocycles of bacteriorhodopsin. Shown are the bR_{568} and bR_{548} photocycles, as well as a possible connection between the two photocycles. Pathways that are not firmly established are shown as dotted lines.

of the resulting simulated model had a RMSD of 2.8 Å from the electron microscopy model structure. A first attempt to place water into bacteriorhodopsin had been made by Zhou et al. (1993). Significant improvements of the simulated bR_{568} structure, reported in Humphrey et al. (1994), resulted from a refinement procedure that included an all-atom force field and hydrogen bonding forces as well as from a renewed attempt to place water molecules inside bR. This refined bR_{568} structure shows close agreement with the Henderson structure (Henderson et al., 1990), the root mean square deviation (RMSD) for the C_α backbone atoms of the membrane-spanning part of bR measuring only 1.8 Å. An explicit representation of all of the hydrogen atoms has also been incorporated into the simulated structure. The most important feature of the refined model is that it reproduces well the interactions in the retinal binding site as observed through reconstitution of bR with retinal analogues. This supports the assumption that structural details at a resolution in the 1-Å range are properly represented, but, of course, there exists a large probability that the structure also contains major faults. The refined model of bR_{568} has been used as a starting point of our simulations of bR_{548}.

The program X-PLOR (Brünger, 1988), with the CHARMm energy function (Brooks et al., 1983) was used for all molecular dynamics simulations reported here. All simulations used a cutoff distance of 8 Å and a dielectric constant of $\epsilon = 1$. All atoms, including hydrogens, are described explicitly. We also use an explicit hydrogen-bonding term in the energy function provided by X-PLOR/CHARMm. The parameters and charges used in the simulations are, respectively, the parma11h3x.pro parameters and the topa11h6x.pro charges (Brooks et al., 1983; Brünger, 1988), except for retinal.

Equilibrium bond lengths, angles, and torsional angles assumed for the retinal chromophore are those determined by recent x-ray crystallography studies (Santasiero and James, 1990). The charges and force constants used for the protonated Schiff base of retinal are those also used in Humphrey et al. (1994).

The protonation states of titratable groups in bR are as given in the standard X-PLOR amino acid topology files, except for Asp-96 and Asp-115, which are assumed protonated according to the observations in Gerwert et al. (1989) and Engelhard et al. (1990). As suggested previously (Bashford & Gerwert, 1992; Zhou et al., 1993), Arg-82 has been moved up to a position facing toward the cytoplasmic side of the protein. In this position, Arg-82 is part of the Schiff base counterion complex. All simulations, except where otherwise stated, were performed at 300 K.

Inducing the light → dark adaptation

The 13-cis,15-syn isomer of bacteriorhodopsin, i.e., of bR_{548}, was simulated through isomerization of in situ retinal around both its C_{13}-C_{14} and its C_{15}-N

bond starting from the simulated model of bR_{568} reported in Humphrey et al. (1994) containing all-trans retinal. Isomerization around these bonds is accomplished through modification of the potential function governing the respective dihedral angles. The potential used in X-PLOR is

$$E_{dihe} = k_\phi [1 + \cos(n\phi + \delta)], \tag{1}$$

where ϕ is the actual torsion angle, k_ϕ is an energy constant, n is the periodicity, and δ is a phase shift. In the electronic ground state, $n = 2$ and $\delta \approx 180°$ are suitable parameters for the conjugated carbon chain of retinal. This implies that each bond can assume either a trans or a cis configuration. The isomerization all-trans,15-anti → 13-cis,15-syn was induced by changing the torsional potential in Eq. 1 for the C_{13}-C_{14} and the C_{15}-N bond such that the all-trans,15-anti configuration became unstable and the 13-cis,15-syn stable. During this procedure the potentials adopted for the C_{13}-C_{14} and the C_{15}-N bond were

$$E_{dihe}^{13-14} = k_\phi^{13-14}[1 - \cos(\phi)]; \qquad E_{dihe}^{15-N} = k_\phi^{15-N}[1 - \cos(\phi)], \tag{2}$$

respectively. These potentials have a maximum at the trans position $\phi = 180°$ and a minimum at the cis position $\phi = 0°$. k_ϕ^{13-14} and k_ϕ^{15-N} were taken to be 2.5 kcal/mole to ensure that the all-trans,15-anti → 13-cis,15-anti transition occurs in a few picoseconds, i.e., rapidly, without, however, increasing the temperature of retinal significantly. The maximum of the new torsional potential is E_{max} (LA → DA) = 5 kcal/mol. The procedure was followed by equilibration at 300 K for 50 ps. The equilibrated retinal-protein system was identified with bR_{548} and served as the starting structure for the study of the photocycle of bR_{548}.

Inducing the photoisomerization

The initial photoisomerization step of the photocycle of bR_{548} was induced by instantaneous change of the torsional potential (Eq. 1) for the C_{13}-C_{14} bond such that the 13-cis configuration became unstable and the respective trans configuration stable. The potential used for this purpose was

$$E_{dihe}^{13-14} = k_\phi^{iso}[1 + \cos(\phi)]. \tag{3}$$

This potential has a maximum at the 13-cis position $\phi = 0°$ and a minimum at the trans position $\phi = 180°$. For k_ϕ^{iso}, a value of 22.5 kcal/mol had been assumed such that the torsional potential at its maximum measures E_{max} (photo) = 45 kcal/mol, i.e., a value close to the energy of a 548-nm photon. The reader should note that this value is much larger than the value of $E_{max} = 5$ kcal/mol(LA → DA) assumed for the transformation from light-adapted to dark-adapted bR.

The primary reaction of the 13-cis photocycle is very fast. The time needed to reach the intermediate J is only 1.2 ps (Zinth et al., 1988). This implies that the crossing between potential energy surfaces of the S_0 and S_1 states of the retinal chromophore occurs close to the maximum of the ground state potential surface (Schulten and Tavan, 1978). It has been suggested that retinal relaxes in ~200 fs (Mathies et al., 1991) to the excited state minimum near the ground state isomerization barrier, with a torsion around the C_{13}-C_{14} bond of ~90°, then crosses to the ground state potential surface and completes the photoisomerization. In our simulations, this process was described by the single potential surface (Eq. 3) that, hence, represents in its higher energy range the excited state potential and, in its lower energy range, the ground state potential. Photoisomerization of the C_{13}-C_{14} bond is achieved by placing the initial 13-cis state at the maximum of the potential (Eq. 3). Subsequent simulations then monitor the relaxation of retinal down the potential surface (Eq. 3). The simulations account for inertial effects as well as for the steric interactions that resist the isomerization enforced by the potential (Eq. 3).

Corotation of the C_{14}-C_{15} bond

We started the simulated photoisomerization from the 13-cis,15-syn retinal configuration. Previous studies (Nonella et al., 1991; Zhou et al., 1993) showed that concomitant rotations around the C_{14}-C_{15} bond can occur and determine the geometry of retinal after the photoisomerization. Because

little is known regarding the excited state torsional barrier for this bond, we carried out simulations with different respective barriers. The potential describing the torsional angle of the C_{14}-C_{15} bond is

$$E_{dihe}^{14-15} = k_{\phi}^{14-15}[1 - \cos(2\phi)], \qquad (4)$$

where the parameter k_{ϕ}^{14-15} is chosen according to the torsional energy barrier desired. In one simulation, we chose a torsional barrier (of the C_{14}-C_{15} single bond) of 2 kcal/mol to enable essentially free rotation around this bond in the excited state such that both the 13-*cis* → all-*trans* and the 13-*cis* → 14-*cis* isomerizations are feasible. In another simulation, we enforced a 13-*cis*, 15-*syn* → 15-*syn* isomerization by assuming a barrier of 10 kcal/mol, preventing rotation around the C_{14}-C_{15} bond:

Sampling photoisomerization processes

In the present work we have addressed also the question of connectivity between the cycles of bR_{548} and bR_{568}. We have explored at which state of the bR_{548} cycle leakage to the bR_{568} cycle might occur. To account for the fact that the probability of leakage between the cycles is smaller than unity we simulated photoisomerization processes for different (random) initial velocities (starting from the same structure of bR_{548}) to account for the possibility that the photoisomerization of bR_{548} might not always involve the same geometrical transformation.

Simulated annealing for the L intermediate

An attempt has been made to simulate the L_{610} state of the bR_{548} photocycle, which is generated within 10 ns. Because such a long time scale is not easily accessible for molecular dynamics simulations we resorted to the so-called simulated annealing technique to model the L_{610} intermediate. Simulated annealing constitutes a systematic technique that has both a solid theoretical foundation (van Laarhoven and Aarts, 1987) and a broad range of successful applications, in particular, in the area of biomolecular structure refinement (Brünger, 1991). Our annealing procedure has encompassed the slow cooling protocol consisting of two steps. First, starting at a temperature of 500 K the protein was cooled down to 300 K through coupling the protein motion to a heat bath by means of the t-coupling method (friction coefficient = 0.1 fs^{-1}) (Berendsen et al., 1984). Every 100 fs the temperature of the heat bath was lowered by 10 K until a final temperature of 300 K was reached. The same procedure was then repeated starting from 400 K. The resulting structure was finally equilibrated for 10 ps at 300 K.

Simulating retinal analogues

Retinal modifications were performed on the equilibrated structure of bR_{548}. The modifications were accomplished with the PATCH facility of X-PLOR; initial coordinates were assigned using the positions of replaced atoms and using the HBUILD command to generate coordinates for explicitly added hydrogens. For all simulations, including retinal analogues, we carried out an energy minimization after the modifications, followed by 5 ps of equilibration and 5 ps of dynamics.

RESULTS

Construction of bR$_{548}$

The refined simulated model of bR_{568} reported in Humphrey et al. (1994), containing all-*trans* retinal, was used as a starting point. In simulation A1, the isomerization from all-*trans*,15-*anti* to 13-*cis*,15-*syn* retinal was enforced as described in Materials and Methods. Fig. 2 presents the dihedral angles of the C_{13}-C_{14} and C_{15}-N bonds during the thermal isomerization. It can be seen that the isomerization is completed after ~2 ps. The results also show that the rotations
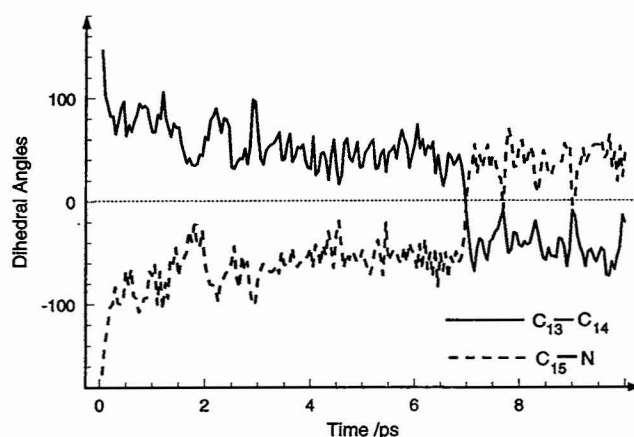

FIGURE 2 Variation of the dihedral angles of the C_{13}-C_{14} and C_{15}-N bonds of retinal during simulation A1.

around the C_{13}-C_{14} and C_{15}-N bonds are strongly correlated with each other; i.e., the sum of the dihedral angles of the C_{13}-C_{14} and C_{15}-N bonds tends to be zero, corresponding to a bicycle pedal motion (Warshel, 1976). Such motion had been suggested for the transition from bR_{568} to bR_{548} in Orlandi and Schulten (1979) on account of a quantum chemical prediction of a low (22 kcal/mole) barrier.

The thermal isomerization described was followed by a 50-ps equilibration (simulation A2). The resulting structure, corresponding to bR_{548}, is depicted in Figs. 3–5. Fig. 3 provides a view of the protein backbone, water, and retinal. The Schiff base region of the proposed structure is shown in Fig. 4, along with a stereo view in Fig. 5. These figures show the relative positions of active groups in the binding site, as well as the suggested positions and orientations of water molecules in this region. Hydrogen bonds are shown as dashed lines together with the associated distances from hydrogen to hydrogen bond acceptor, to judge the strength of the respective bonds. The hydrogen bonds, near the Schiff base nitrogen, form a network involving five proximate and two distant water molecules and protein residues Asp-85, Asp-212, Arg-82, Tyr-185, and Tyr-57. The oxygens of Asp-85 are located at an average distance of 5.6 Å and 5.0 Å from the Schiff base hydrogen, whereas both oxygens of Asp-212 are at a distance of ~4.2 Å (Fig. 6 a). Two water molecules connect the Schiff base NH to the carboxylate of Asp-85. Asp-212 is strongly hydrogen bonded to Arg-82, Tyr-57 (through a water molecule), Tyr-185, and Trp-86 (not shown) and to a water molecule. The picture is similar to the binding site of the simulated model of bR_{568} (Humphrey et al., 1994) in which Asp-212 is hydrogen bonded to various protein residues in contrast to Asp-85, which is connected only to Arg-82. Tyr-57, besides being connected to Asp-212 through a water molecule, is connected as well to Asp-85 and Arg-82 through other water molecules.

Fig. 6 presents some dynamical properties of the suggested bR_{548} model. Fig. 6 a shows the distances of the carboxylate oxygens of residues Asp-85 and Asp-212 to the Schiff base proton during the last 5 ps of equilibration. Asp-212 is seen
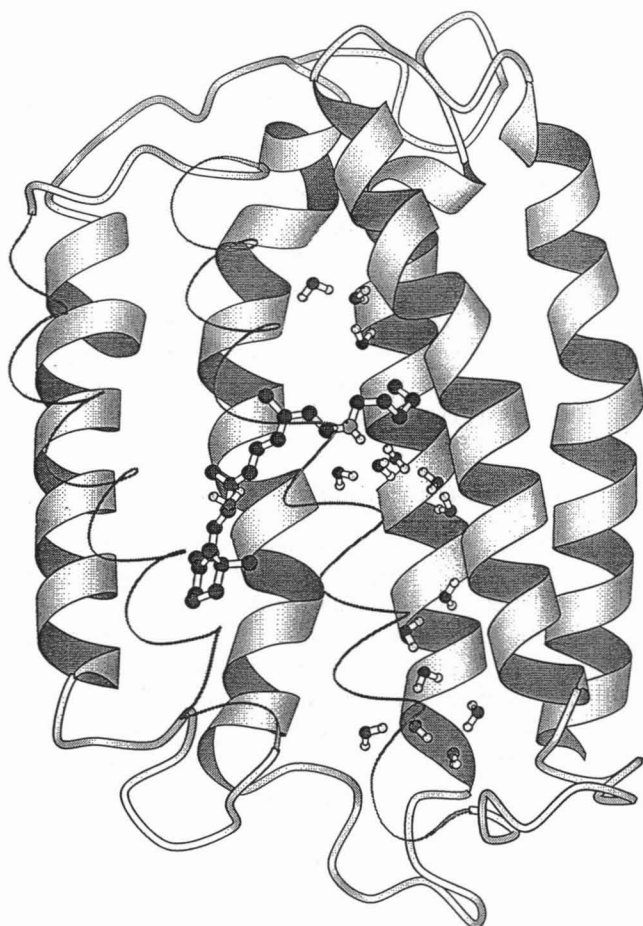
FIGURE 3   Ribbon diagram of bR$_{548}$, including retinal and water molecules, generated with MOLSCRIPT (Kraulis, 1991). Helices C and D are shown as thin lines to reveal the protein interior.
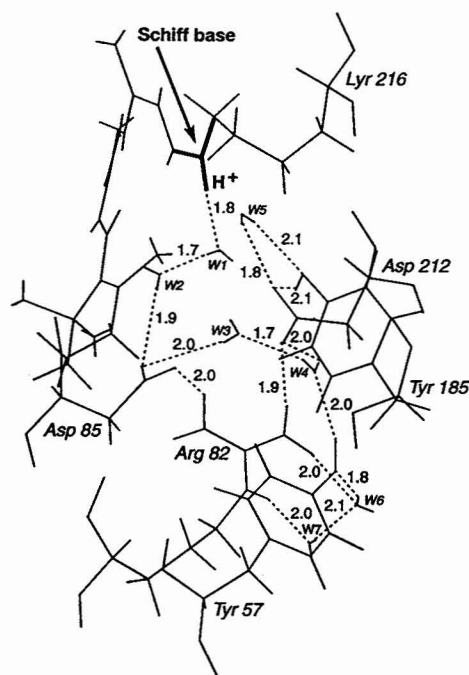

FIGURE 4   View of the retinal binding site, showing positions of water molecules, important residues, and distances of hydrogen bonds.

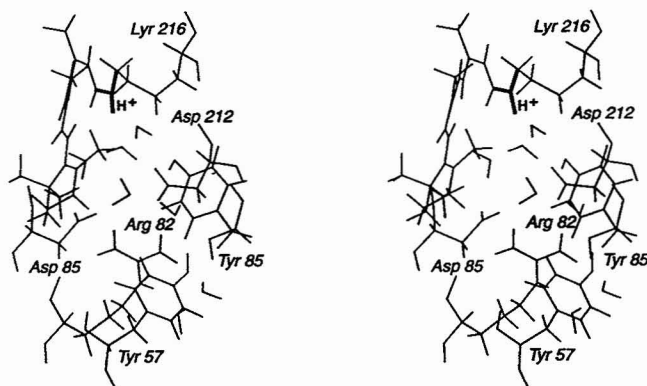FIGURE 5   Stereo view of the retinal binding site.

to remain rather immobile, with both oxygens maintaining a distance of ~4.2 Å. Asp-85 exhibits larger fluctuations, but its motion is still relatively small, with distance values of 4.6 and 5.6 Å for the two oxygens. The relative immobility of residues Asp-85 and Asp-212 provides a good indication of the stability of retinal's counterion complex in the simulated model.

Similar to the bR$_{568}$ model (Humphrey et al., 1994), the bR$_{548}$ model suggested here exhibits a distinctive twist of retinal's backbone. The overall twist of 55° is a result of torsions around retinal's single bonds. The largest twist of 30° is observed around the C$_{12}$-C$_{13}$ bond. Fig. 6 b presents the fluctuations of the dihedral angles of the C$_6$-C$_7$, C$_{10}$-C$_{11}$, and C$_{14}$-C$_{15}$ bonds during the last 5 ps of simulation A2. It should be noticed that fluctuations increase going toward the β-ionone ring. Fluctuations of the C$_{14}$-C$_{15}$ torsion are very small; this bond stays essentially planar. The C$_6$-C$_7$ torsion angle, which determines the rotation of the β-ionone ring relative to the retinal plane, is seen to fluctuate in a wide range of angles, deviating up to 60° from the planar conformation, around an average value of 20°.

An interesting difference between bR$_{568}$ and bR$_{548}$ emerged in the vibrational spectra observed by Fourier trans-

form infrared (Roepe et al., 1988), Fourier transform Raman (Sawatzki et al., 1990), and resonance Raman (Smith et al., 1987; Noguchi et al., 1990) spectroscopy. bR$_{548}$ exhibits stronger intensities of the C$_{14}$-H hydrogen-out-of-plane modes than bR$_{568}$. This difference had been attributed to a twist of the C$_{14}$-C$_{15}$ bond in bR$_{548}$. Our results do not support this explanation. The C$_{14}$-C$_{15}$ bond is found to be planar. However, we find a strong steric interaction between the hydrogen on C$_{14}$ and the two hydrogens on C$_\epsilon$ of the Lys-216 side chain (see Fig. 11).

Additional differences between bR$_{568}$ and bR$_{548}$ have been observed in solid-state nuclear magnetic resonance (NMR) spectroscopy (Smith et al., 1989). First, the chemical shifts of ^{13}C$_{13}$ and ^{13}C$_{15}$ in the case of bR$_{568}$ is further upfield than in the case of bR$_{548}$. Second, the opposite holds for ^{13}C$_{14}$, which exhibits an upfield chemical shift for bR$_{548}$ relative to
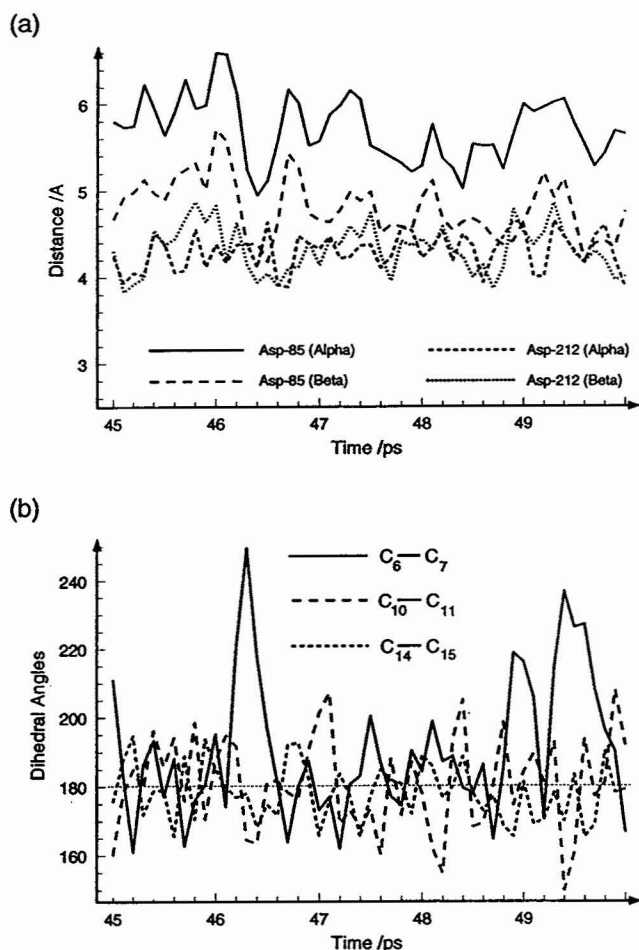
(a)

(b)

FIGURE 6 (a) Distances between oxygen atoms of Asp-85 and Asp-212 to the Schiff base proton, during the last 5 ps of simulation A2. (b) Dihedral angles, designated by their respective bonds, of retinal during the last 5 ps of simulation A2.

bR_{568}. The first difference has been explained by a stronger interaction between the Schiff base and the associated counterions. This explanation is corroborated by our simulations presented here and in Humphrey et al., (1994), which suggest that in bR_{548} the carboxylate moieties of Asp-85 and Asp-212 are closer by ~1 Å to the Schiff base as compared with bR_{568}. Studies with model compounds indicated as well that stronger electrostatic interactions between the positively charged Schiff base linkage and its counterion induces downfield shifts in the $^{13}C_{13}$ NMR (Albeck et al., 1992). It had been suggested that the second difference results from steric interactions between $C_{14}H$ and the $C_\epsilon H_2$ of Lys-216. This explanation is also in harmony with our results reported here and in Humphrey et al. (1994) in that we find for bR_{548} a close proximity (2.8 Å) between C_{14} and C_ϵ. The upfield shift that was measured by $^{13}C_{14}$ NMR is much stronger than that observed in model compounds (Livnah and Sheves, 1993). This difference can originate from a twist around the C_{14}-C_{15} bond that the 13-cis,15-syn retinal protonated Schiff base experiences in solution but that is prevented in the protein. A twist around the C_{14}-C_{15} bond should weaken the interaction be-

tween $C_{14}H$ and the $C_\epsilon H_2$ of Lys-216, thereby reducing the upfield shift effect observed in the $^{13}C_{14}$ NMR spectrum.

Examination of the structure of bR_{548}

Various experimental data concerning the spectral properties of bR reconstituted with different 13-cis-retinal analogues are available (Sheves et al., 1984). In addition, in several artificial pigments (Steinberg et al., 1991) as well as in some mutants of bR, the ratio of all-trans,15-anti and 13-cis,15-syn retinal in light-adapted and dark-adapted bR has been determined. These observations can be used to check the validity of the suggested bR_{568} and bR_{548} structures.

Simulation of the D85A mutant

It was observed by resonance raman studies (Rath et al., 1993) that mutation of Asp-85 to alanine significantly lowers the $C = N$ stretching frequency of the protonated Schiff base in bR_{548} from 1642 cm^{-1} to 1616 cm^{-1}. This effect is accompanied by an unusually small deuterium effect (6 cm^{-1}) on the $C = N$ stretching frequency. Both effects can be attributed to weak hydrogen bonding to the Schiff base NH group prevailing in this mutant of bR_{548}. It is currently believed that the $C = N$ stretching frequency is significantly controlled by its coupling with N/H bending, and a weak hydrogen bonding to NH will induce a lower $C = N$ stretching frequency (Aton et al., 1980; Kakitani et al., 1983; Baasov et al., 1987). In native bR, the $C = N$ stretching frequency of both trans and 13-cis isomers is similar, pointing to a similar environment of the N-H bond. However, the resonance raman experiment suggests quite a different environment in D85A mutants of these isomers.

Simulation B1 modeled the effect of an Asp-85 → Ala mutation. Residue modification was followed by a 10-ps equilibration of the protein. A detailed picture of the mutant active site is given in Fig. 7. A comparison of Figs. 4 and 7 reveals considerable changes in the active site of the D85A mutant as compared with native bR_{548}. Structural changes not only involve the nearest neighbors of Ala-85 but also extend over the whole binding site. The hydrogen-bonding network within the active site is completely modified. It is suggested that the hydrophilic groups surrounding the binding site are no longer bridged together to form an integrated counterion complex of the Schiff base; instead, the hydrogen-bonding network of the mutant consists of a few water molecules that, together with Asp-212, form an isolated hydrogen-bonding cluster. The mutation affects the protein backbone as well. The backbone of helix G is found to be distorted from a standard α-helical configuration, with the carbonyl of Asp-212 lacking the usual hydrogen-bonding pattern within the helix. This carbonyl is hydrogen bonded to water molecule W5, which breaks the standard hydrogen bond between the CO group of Asp-212 and the NH group of Lys-216. The most distinctive feature of the simulated D85A mutant model is that there is a very weak hydrogen bonding of the Schiff base NH group to a water molecule. This hydrogen bonding
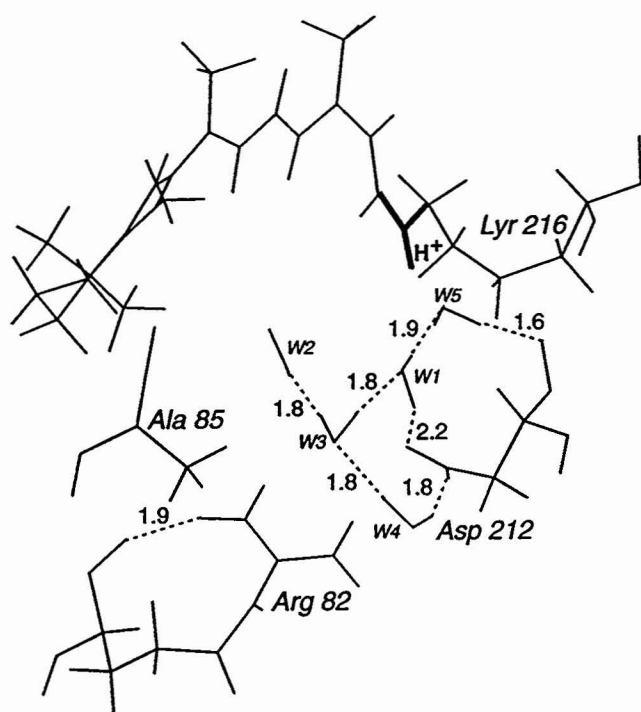
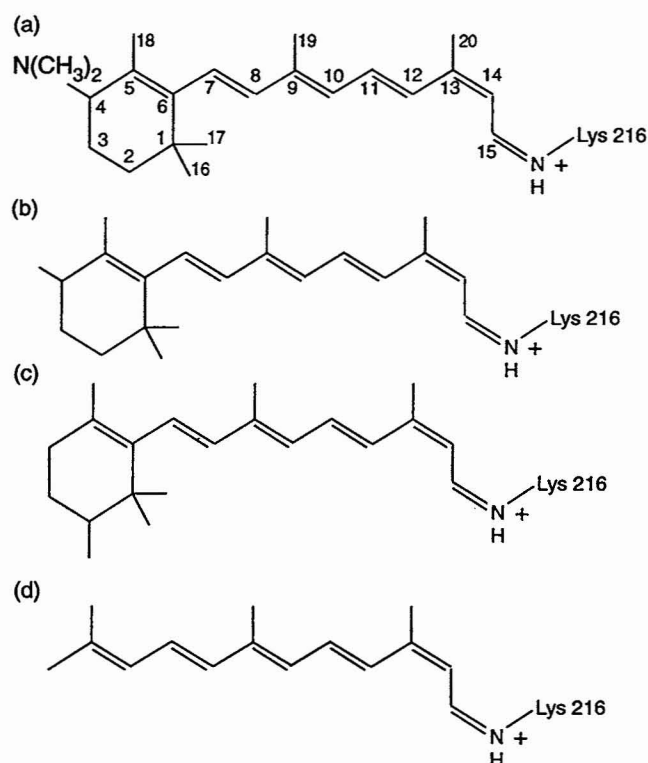FIGURE 7   Retinal binding site for the D85A mutant.

FIGURE 8   Retinal analogues investigated: (a) 4-dimethylamino analogue and numbering scheme of retinal atoms; (b) 4-methyl analogue; (c) 2-methyl analogue; and (d) cleaved-ring analogue.

is weaker than that observed in the model of bR_{548} and provides an explanation for the low C=N stretching frequency and the small deuterium effect observed in the resonance raman studies of bR_{548} mutant D85A. Simulations of the D85A mutant of bR_{568} (not shown) indicate only minor changes in the hydrogen bonding strength of water molecule to the NH moiety for the mutant, in keeping with the resonance raman results that show a moderate shift in the C=N stretching frequency from 1642 cm^{-1} to 1630 cm^{-1} (Rath et al., 1993).

Retinal analogues simulations

Experiments with modified retinal chromophores have proven to be a powerful tool for obtaining information on the steric interactions of retinal with the surrounding protein environment (for review see Ottolenghi and Sheves, 1989). In the present study we focus on the retinal β-ionone ring modifications, which provide clues for orientation and location of the retinal ring within the binding site. Fig. 8 presents the four retinal analogues considered. Studies of artificial pigments derived from the retinal analogues reveal that introduction of bulky substituents at the ring C_4 position blue-shifted the absorption maximum of both trans and 13-cis isomers of bacteriorhodopsin considerably (Sheves et al., 1984; Steinberg et al., 1991). In contrast, a methyl substitution at the C_2 position do not cause any significant change in the absorption maximum (Sheves and Friedman, unpublished results). Simulations of the artificial pigments derived from the analogues depicted in Fig. 8 and comparison with the spectral shifts observed for the respective pigments should provide a

measure of the consistency and accuracy of the simulated bR_{548} model suggested here. Results of these simulations are given in Fig. 9.

4-Dimethylamino modification

Simulations C1A and C1B were carried out to determine the effect of substitution of the retinal C_4 position with a dimethylamino group (Fig. 8 a) and resulted in two structures, bR_{C1A} and bR_{C1B}. The two structures arise as the C_4 position has two hydrogen atoms and, thus, there are two possibilities for attachment that are inequivalent as a result of the protein chiral discrimination. We define the plane of retinal facing toward the extracellular side as α and that facing to the cytoplasmic side as β. bR_{C1A} corresponds to the retinal analogue substituted at the α-position and bR_{C1B} to substitution at the β-position.

Fig. 9 a summarizes the results of the simulations of bR_{C1A} and bR_{C1B}. Shown in this figure are the torsional angles of bonds along the retinal backbone. For the native pigment, retinal is in a 13-cis,15-syn configuration, with the C_6-C_7, C_8-C_9, C_{10}-C_{11}, and C_{12}-C_{13} bonds slightly twisted, giving rise to the corkscrew configuration of retinal in the simulated bR_{548} model discussed above. The changes of retinal's conformation in going from bR_{548} to bR_{C1A} are quite noticeable. Substitution of the C_4 α-position by a dimethylamino group leads to a considerable twist of 20° around the C_{13}-C_{14} double bond (rotation barrier, 20 kcal/mol) and around the C_{14}-C_{15}
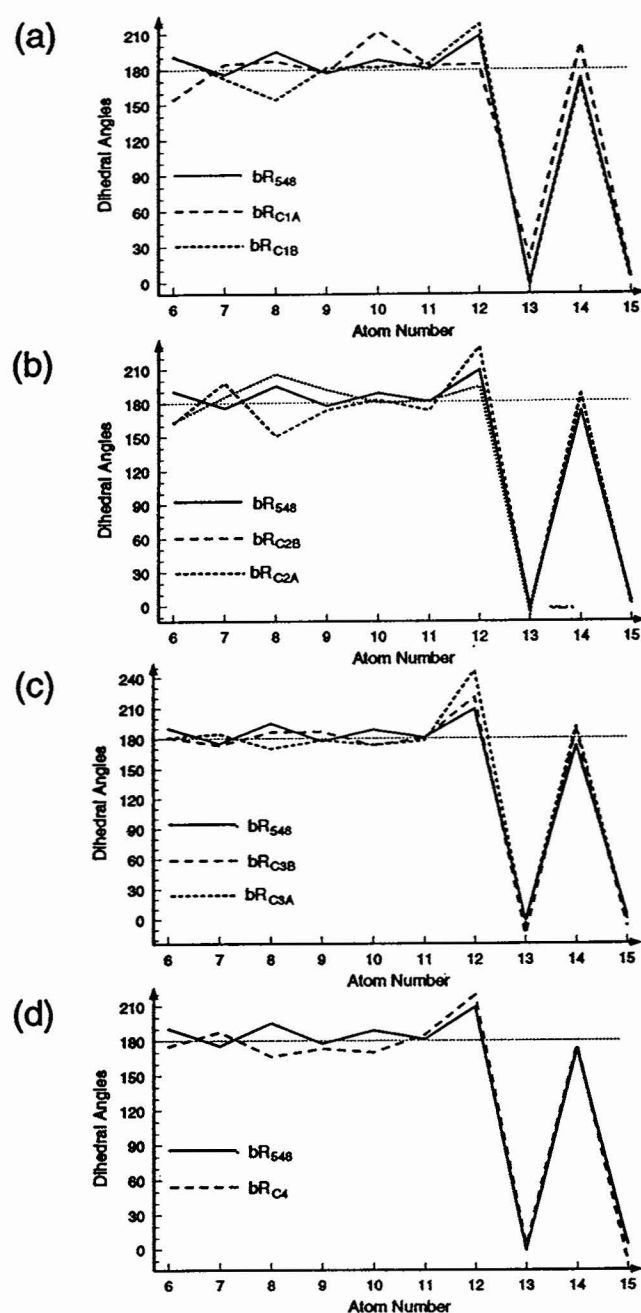
FIGURE 9   Comparison of dihedral angles along retinal's backbone for the retinal analogues shown in Fig. 8: (a) 4-dimethylamino analogue; (b) 4-methyl analogue; (c) 2-methyl analogue; and (d) cleaved-ring analogue.

The C_4 positions of retinal are achiral; however, after incorporation into the protein binding site, the two enantiomers are different, and chiral discrimination by the protein is possible. Thus, in general, substitution at the C_4 position should result in two different enantiomers that one, indeed, often observed through two spectral maxima of the reconstituted bR (Ottolenghi and Sheves, 1989). When a single spectral maximum is observed, one expects only one enantiomer to reconstitute. When bR is reconstituted with 13-*cis*,15-*syn* retinal with a dimethylamino group at the C4 position, a single pigment absorbing at 460 nm is observed (Sheves *et al.*, 1984). We suggest that this absorption corresponds to the simulated bR_{C1B} pigment. The large degree of the retinal twist caused by the β-position substitution could explain the blue-shifted 460-nm peak. The considerable twist of the double bonds and overall shift of the retinal molecule observed for bR_{C1A} indicates that binding of the dimethylamino group to the α-position requires a conformational change, too large to allow this retinal analogue to reconstitute with bacteriorhodopsin. The proximity of Trp-138 prevents attachment of the bulky dimethylamino group to the α-position, but this group can be accommodated at the β-position at the price of some twists in retinal.

4-Methyl modification

Simulations C2A and C2B modeled the effect of methyl group substitutions at the C_4 position of retinal (Fig. 8 *b*) and resulted in the simulated structures bR_{C2A} and bR_{C2B}. Attachment at the α-position corresponds to bR_{C2A}, attachment at the β-position corresponds to bR_{C2B}. The results of the simulations are summarized in Fig. 9 *b*. In the case of bR_{C2A}, the system stays very close to the bR_{548} conformation. Slight rotations around different bonds essentially compensate each other, leaving the overall geometry and orientation of retinal virtually unchanged. The retinal geometry and orientation in the case of bR_{C2B} are quite different from that in bR_{548}. The C_8-C_9 bond rotates by 45° from the original conformation, developing the twist with absolute value of 30°. The C_{12}-C_{13} bond develops an even larger twist of 50°. It is suggested that these major rotations around two single bonds lead to a retinal conformation that is noticeably more twisted as compared with the native chromophore.

Experimental studies with artificial pigments revealed that substitution of a methyl group at the C_4 position resulted in two pigments, which absorbed at 550 and 460 nm (Ottolenghi and Sheves, 1989). A possible explanation for the two observed pigments is that each pigment consists of a different enantiomer. The fact that bR_{C2B} contains very large rotations about retinal's single bonds, particularly about the C_8-C_9 and C_{12}-C_{13} bond, suggests that the respective enantiomer corresponds to the strongly blue-shifted 460-nm peak. The simulated bR_{C2A} model shows very little conformational change from the native pigment model and suggests that the corresponding enantiomer produces the 550-nm peak. The close proximity of Trp-138 to the α-position of the C_4 (3.4 Å from the $C_{\delta1}$ atom of Trp-138 to the α-hydrogen

single bond (rotation barrier, 10 kcal/mol); moreover, the simulations suggest that retinal as a whole is shifted by 2 Å in the direction of the Lys-216 backbone. In the case of bR_{C1B}, the resulting conformation shows some change relative to bR_{548}, but the changes are not as dramatic as in the case of bR_{C1A}. The main difference between the bR_{548} model and bR_{C1B} are in the C_8-C_9 and C_{12}-C_{13} torsional angles. The rotation around the C_8-C_9 bond measures ~25°, and the rotation around the C_{12}-C_{13} bond measures ~40°. Both rotations are approximately 10° larger than those seen in the simulated bR_{548}.

of C_4) could account for this effect, namely, that substitution at the α-position results in a steric hindrance that causes a twist in retinal, whereas substitution at the β-position does not lead to strong steric interactions.

2-Methyl modification

Methyl group substitutions at the C_2 position of retinal resulted in the simulated models bR_{C3A} and bR_{C3B} (Fig. 8 c). As for the previous analogues, bR_{C3A} corresponds to an attachment at the α-position and bR_{C3B} to an attachment at the β-position. Fig. 9 c summarizes the results of the respective simulations. No significant changes in the dihedral angles of retinal's backbone are found in this case, which is consistent with the observation that the spectra are not affected in these analogues. bR_{C3B}, in particular, has a retinal conformation essentially identical with that of the simulated bR_{548} model. In the case of bR_{C3A}, the only significant change is an additional rotation of the C_{12}-C_{13} single bond by 27° relative to its twist in the native pigment. However, it is proposed that this additional twist is offset by smaller rotations around the C_6-C_7, C_8-C_9, and C_{10}-C_{11} single bonds in the opposite direction. Thus, the overall retinal conformation in the case of bR_{C3A} also stays close to that of bR_{548}.

Ring cleavage modification

Simulations were carried out to model the effect of cleaving the ring between the 3- and 4-carbons and between the 1- and 6-carbons, resulting in structure bR_{C4} shown in Fig. 8 d. The resulting dihedral angles of retinal's backbone are summarized in Fig. 9 d. The retinal chromophore, in the case of bR_{C4}, is found to be essentially unaltered as compared with the simulated native pigment. It is suggested that slight rotations around different single bonds induced by the ring cleavage counterbalance each other. The overall retinal shape stays practically unchanged. Results of our simulations are in keeping with a slightly blue-shifted absorption maximum of 535 nm observed for the pigment.

Simulation of the bR₅₄₈ photocycle

Primary photoisomerization

We simulated the initial photoisomerization step of the bR_{548} photocycle by instantaneously changing the torsional potential of the C_{13}-C_{14} bond as described in Materials and Methods. We carried out three simulations, simulations D1 and D3 with a torsional barrier of 10 kcal/mol for the C_{14}-C_{15} single bond and simulation D2 with a barrier of 2 kcal/mol for this bond. All simulations were started from the 13-*cis*,15-*syn* configuration of retinal and lasted 1 ps. The resulting simulated structures were both equilibrated for 10 ps using the torsional potentials for retinal in the ground state. Simulations D1 and D2 were carried out at 300 K, whereas simulation D3 was carried out at 77 K.

Fig. 10 a presents the time dependence of the dihedral angles of the C_{13}-C_{14}, C_{14}-C_{15}, and C_{15}-N bonds during simu-
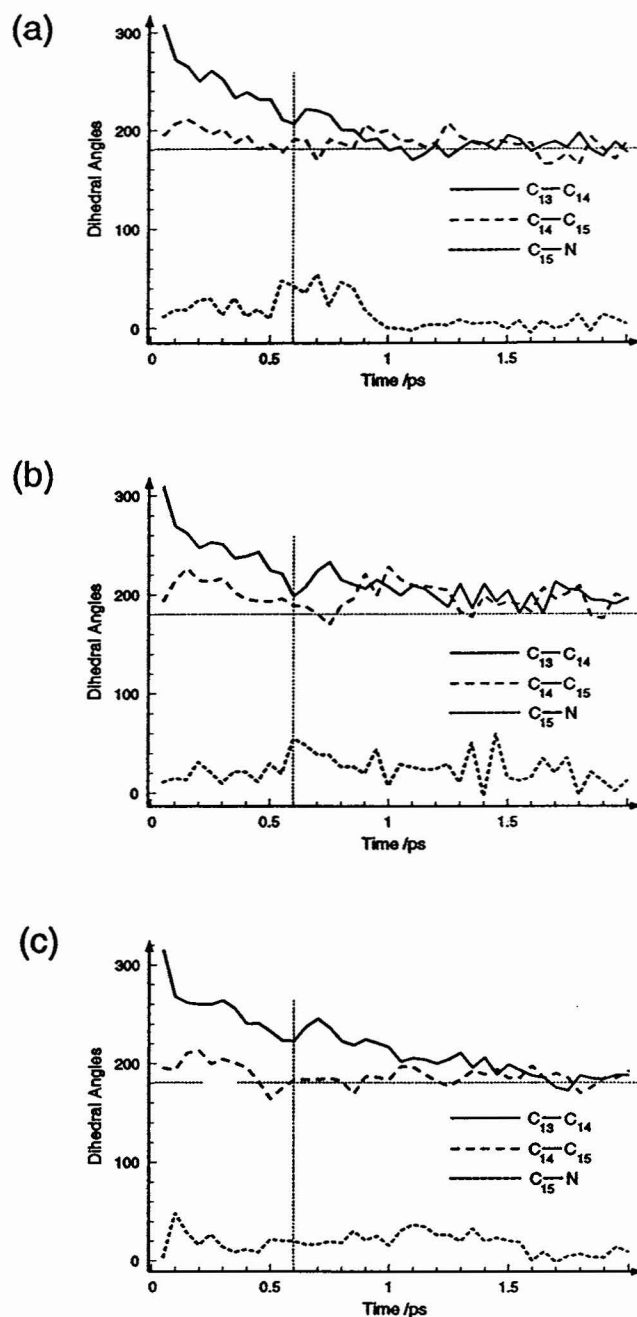
FIGURE 10 Variation of the dihedral angles of the C_{13}-C_{14}, C_{14}-C_{15}, and C_{15}-N bonds of retinal during simulation D1 (a) and D2 (b). A torsional barrier of 10 kcal/mol for the C_{14}-C_{15} bond has been chosen in simulations D1 and D3. A torsional barrier of 2 kcal/mol for the C_{14}-C_{15} bond has been chosen in simulation D2. Simulations D1 and D2 have been carried out at 300 K; simulation D3 has been carried out at 77 K.

lation D1. One observes that the whole isomerization process can be divided into two stages. During the first stage, which lasts ~0.6 ps, retinal isomerizes around the C_{13}-C_{14} bond by ~150°. The simulated bR structure produced after 0.6 ps of the photoisomerization is ascribed to a J intermediate. The strain in the binding site of retinal, caused by the photoisomerization, is further relaxed during the next picosecond of the molecular dynamics simulations when retinal rotates

by another 30° around the C_{13}-C_{14} bond. The simulated structure obtained after this relaxation is assigned to a K_{590} intermediate. In this model the retinal protonated Schiff base proton points up towards the cytoplasmic side of a membrane, with the Schiff base hydrogen forming a hydrogen bond with a water molecule on the cytoplasmic site of the Schiff base linkage. The occurrence of two different kinetics for the dihedral dynamics in our simulations appears in agreement with the observation of an early J intermediate and a later K intermediate in a 13-cis cycle (Zinth et al., 1988).

Fig. 10 b presents the time dependence of the dihedral angles for simulation D2. No essential difference is observed between the simulations D1 and D2 for the behavior of the dihedral angles of the C_{13}-C_{14}, C_{14}-C_{15}, and C_{15}-N bonds. Even though the rotation around the C_{14}-C_{15} bond in the case of simulation D2 has only a 2 kcal/mol barrier, no corotation around this bond is observed. Apparently, the corotation is prevented through steric hindrances due to the *syn* configuration of the C_{15}-N bond. This behavior is distinctly different from that found in the simulated bR_{568} photocycle in which a corotation around the C_{14}-C_{15} bond is possible and arises, in fact, in the case of low respective barriers (Nonnela et al., 1991; Zhou et al., 1993; unpublished results).

J intermediate

The simulated structure obtained after 0.6 ps of the photoisomerization process is defined here as that of the J intermediate. In our simulations this intermediate is unstable and converts to a new intermediate (see below) as a result of torsions of retinal's double bonds and a lack of hydrogen bonding stabilizing the momentary position of the protonated Schiff base, structural features that can be discerned from Fig. 11. The dihedral angles of retinal's backbone in the simulated model are shown in Fig. 12. This figure suggests that the C_{13}-C_{14} bond is twisted by 25° and the C_{15}-N bond is twisted by 45°; these strong torsions explain the lack of stability as well as the resonance raman spectra that suggest that the retinal chromophore is twisted (Noguchi et al., 1990).

K_{590} intermediate

Our simulations suggest (Fig. 10) that, in ~1.2 ps after photoisomerization, retinal's dihedral angles assume essentially stationary values corresponding to an intermediate with a retinal all-*trans*,15-*syn* geometry that is stable on the time scale (20 ps) of the simulation. We identify this state with the K_{590} intermediate that is observed experimentally within 3 ps after light absorption (Zinth et al., 1988). The proposed model of the intermediate is presented in Fig. 11. The Schiff base NH group points to the cytoplasmic side and engages in hydrogen bonding with a nearby water. Figs. 11 and 12 show that the backbone of retinal in the K_{590} state is torsionally more relaxed than the J intermediate. The suggested geometry is consistent with the blue shift of the spectrum of K_{590} with respect to the spectrum of J. The absorption maxi-
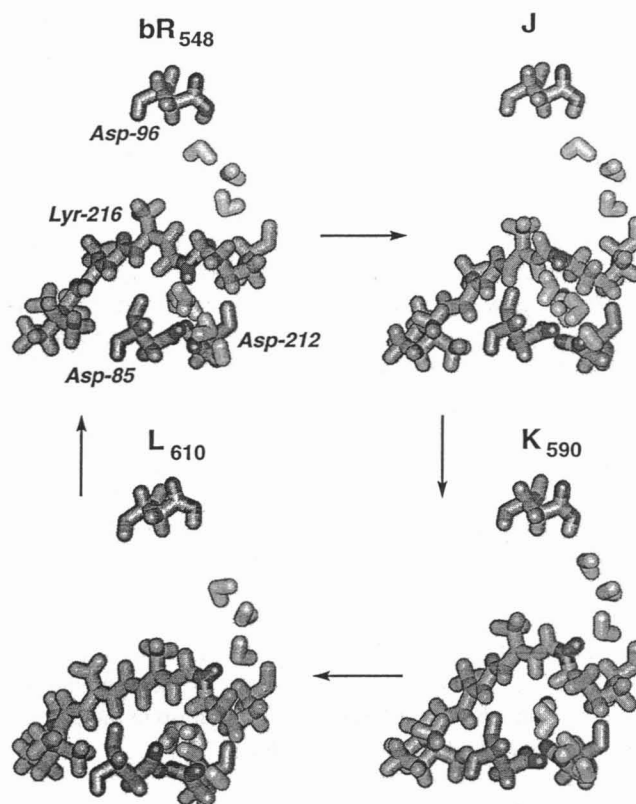

FIGURE 11 Intermediates of the 13-*cis* photocycle. Shown are the retinal molecule bound to a lysine side chain, three aspartic acids that play an important role in the photocycle, and the water molecules at the binding site.
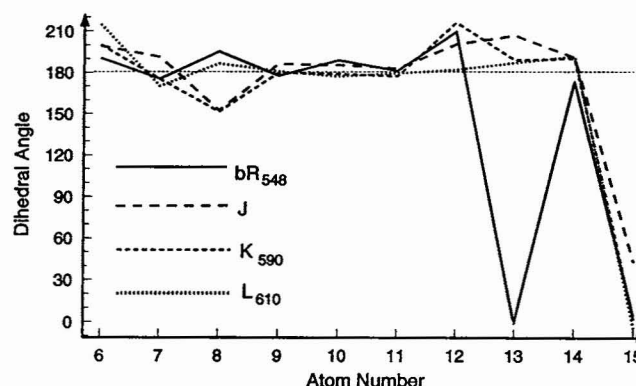

FIGURE 12 Comparison of dihedral angles along retinal's backbone for the intermediates shown in Fig. 11.

mum, however, is more red-shifted than the spectrum of the in initial bR_{548}, a property that can be attributed to the larger separation between the protonated Schiff base and the negatively charged Asp-85 and Asp-212 residues (see Fig. 11). The torsional angles given in Fig. 12 indicate that K_{590} in the vicinity of the bonds C_6-C_9 and C_{12}-C_{13} is considerably less planar than bR_{548}; this result is consistent with the observation of strong hydrogen-out-of-plane bands for K_{590} (in a 13-*cis* photocycle of an artificial pigment derived from a 13-demethylretinal) as reported in Noguchi et al. (1990).

L_{610} intermediate

Application of the annealing scheme described in Materials and Methods leads to convergence to a third structure that is presented in Figs. 11 and 12. Assuming that the annealing scheme effectively bridges a longer time scale, we interpret this structure as the L_{610} intermediate that is observed to form within 5 ns after light absorption. The dihedral angles proposed by our simulations for L_{610} in Fig. 12 show that the retinal chromophore at the L_{610} stage is essentially planar, a feature that contributes to a red-shifted spectrum relative to the spectrum of K_{590}. We note that the spectrum of this late nanosecond intermediate of the bR_{548} cycle is significantly red-shifted relative to the spectrum of the late microsecond intermediate of the bR_{568} photocycle, i.e., of L_{550}. In addition to the larger torsions observed in the molecular dynamics simulations of the L_{550} structure (unpublished results), the main difference between the two intermediates is the direction in which the N-H bond points. In L_{610} of the bR_{548} photocycle, the N-H bond points to the cytoplasmic side, which results in a larger distance between the protonated Schiff base and Asp-85 and Asp-212. Our results suggest that this large distance is the major cause for the red shift in L_{610}.

Fig. 11 shows clearly that the simulated L_{610} intermediate features a protonated Schiff base with its proton pointing towards the cytoplasmic side, participating in a hydrogen bond network on this side, and not engaging in any hydrogen bonding to Asp-85 or Asp-212. This result provides an explanation for the fact that an unprotonated intermediate, i.e., an M intermediate, is not formed in the bR_{548} photocycle; instead of passing through an unprotonated intermediate, the bR_{548} cycle decays back from L_{610} to bR_{548} with a halftime of 40 ms (Kalisky et al., 1977; Hofrichter et al., 1989). We note that an M intermediate was observed in the photocycle of bR_{548} measured at pH values higher than 9 (Drachev et al., 1993) and in an artificial pigment derived from 13-demethyl,14-F retinal (Steinberg et al., submitted for publication). It is possible that both cases induce a different isomerization or have different proton transfer pathways.

Low temperature isomerization

Many experimental studies of the bR_{548} photocycle were conducted at low temperatures (Iwasa et al., 1981; Roepe et al., 1988; Balashov et al., 1991). We have carried out, therefore, a simulation of the bR_{548} photoisomerization at $T = 77K$. The resulting motion of the dihedral angles during the first 2 ps of the photocycle are presented in Fig. 10 c. Similar to the cycle at $T = 300$ K, the dihedral angle of the C_{13}-C_{14} bond rotates by 140° within ~0.5 ps. However, the remaining rotation of this bond by 40° requires ~1.5 ps, which is noticeably slower than the relaxation of this angle in the $T = 300$ K case. As kinetics of the J to K transition is temperature dependent, this transition appears to be thermally activated. Formation of the J intermediate is observed to be temperature independent and can be considered as a purely photochemical process.

Leakage from 13-*cis* to the *trans* cycle

Bacteriorhodopsin in the dark is found to form a mixture of bR_{568} and bR_{548} in a 1:2 ratio. After exposure to light, bR is found only in the bR_{568} state. This conversion has been attributed to a leakage from the bR_{548} cycle to the bR_{568} cycle, every absorption of a photon by bR_{548} leads with approximately 10% probability to bR_{568} (Korenstein and Hess, 1977). A number of pathways had been proposed for the light adaptation, with various steps of the 13-*cis* photocycle as possible branching points (Sperling et al., 1977; Kalisky et al., 1977; Sperling et al., 1979; Iwasa et al., 1981; Varo and Bryl, 1988; Bryl et al., 1992). It is conventionally assumed that the leakage occurs during the post-K stages of the bR_{548} cycle through a 15-*syn* → 15-*anti* isomerization leading directly to bR_{568}. Here we investigate another leakage pathway that involves a 13-*cis*,15-*syn* → all-*trans*,15-*anti* photoisomerization. For this purpose we lowered, by a small margin, namely 2.5 kcal/mol, the isomerization barrier of the C_{15}-N bond as described in Materials and Methods. Sampling 10 photoisomerization processes (see Materials and Methods), we found that in 7 cases an isomerization to the J and K states occurs as described above, but in 3 cases a 13-*cis*,15-*syn* → all-*trans*,15-*anti* isomerization took place. The time evolution of the dihedral angles for 3 sample cases is presented in Fig. 13, in which case c corresponds to a leakage reaction. These findings suggest the possibility that light adaptation of bR involves a 13-*cis*,15-*syn* → all-*trans*,15-*anti* photoisomerization. It is interesting to observe in Fig. 13 c that the rotation around the C_{15}-N bond occurs essentially after the rotation around the C_{13}-C_{14} bond is nearly completed. We note that similar simulations that were carried out for the all-*trans* photocycle did not lead to coisomerization of the C=N bond.

DISCUSSION AND CONCLUSIONS

Before the present investigation was undertaken, the retinal isomeric state of bR_{548} was already well known, namely, 13-*cis*,15-*syn* (Harbison et al., 1984; Smith et al., 1984; Livnah and Sheves, 1993). One expected that this retinal isomer would fit well into the binding site. However, the detailed conformation of retinal in bR_{548} and its effect on the counterion complex were uncertain. The photocycle of bR_{548} had been studied as well, but it was not understood why bR_{548} does not pump protons. Our simulations allowed us to address these issues. Below we discuss first the properties of the structure of bR_{548} and then its photocycle.

Structure of bR_{548}

Bacteriorhodopsin in the bR_{568} state in the dark converts within ~30 min to the bR_{548} state, assuming a 1:2 equilibrium between the bR_{568} and the bR_{548} forms (Ohno et al., 1977). This contrasts with the behavior of retinal in solution in which a *trans* configuration is more stable (Sheves and
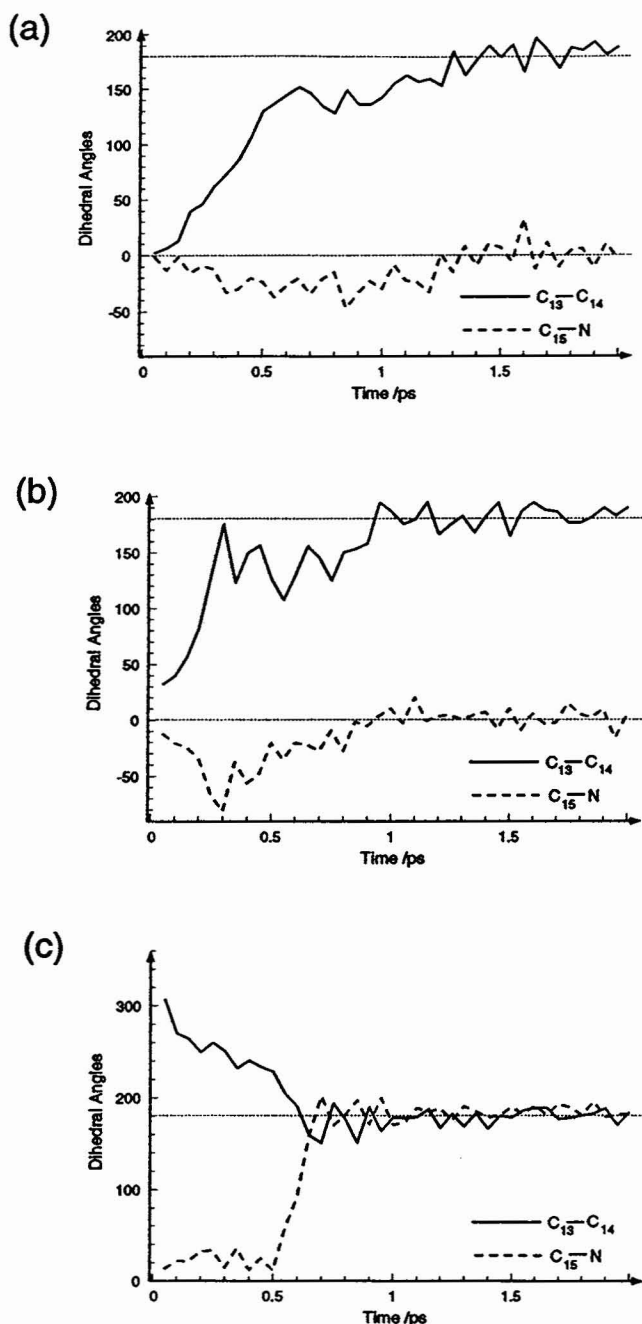
FIGURE 13 Variation of the dihedral angles of the C_{13}-C_{14} and C_{15}-N bonds of retinal during three sample cases of the photoisomerization process.

Baasov, 1984). Obviously, the retinal binding site of bR stabilizes the 13-*cis*,15-*syn* geometry of bR_{548}. The observed stabilization appears to be consistent with the simulated model of bR_{548} presented in Figs. 4 and 5. The simulations suggest that for bR_{548} the distances between the Schiff base hydrogen and the most proximate oxygens of Asp-85 and Asp-212 are ~4.6 and 4.2 Å, respectively, whereas in the simulated model of bR_{568} these distances were suggested to be 5.5 and 4.5 Å (Humphrey et al., 1994). The difference suggests that the spectrum of bR_{568} is shifted to the blue upon transformation to bR_{548}.

The spectral (NMR, vibrational, electronic) differences between bR_{568} and bR_{548} have been mainly ascribed to the twist of the C_{14}-C_{15} bond (Smith et al., 1987, 1989; Roepe et al., 1988; Sawatzki et al., 1990; Noguchi et al., 1990). However, our simulations suggest another explanation. A torsion around the C_{14}-C_{15} bond does not arise; rather, the simulations suggest that the differences between bR_{568} and bR_{548} are the result of the distance between the protonated Schiff base linkage and Asp-85 and Asp-212 as well as the result of different steric interactions between C_{14}-H and C_{ϵ}-H_2 of Lys-216. The simulations also relate successfully to the outcomes of experiments in which bacteriorhodopsin is reconstituted with various analogues of 13-*cis* retinal (Ottolenghi and Sheves, 1989). We conclude from this that the binding site of the ring moiety, possibly also a larger part of the site, is reproduced in our simulations with an accuracy of ~1 Å.

A particularly promising source of information on the properties of dark-adapted bacteriorhodopsin are artificial pigments, mutants, and different wildlife forms (Mukohata et al., 1991) that show vastly different ratios of all-*trans* and 13-*cis* retinal after dark adaptation. As a first step to study such effects, we have investigated the D85A mutant. Resonance raman measurements of the C=N stretching frequency of this mutant indicate a weakened, relative to bR_{548}, hydrogen bonding of the Schiff base linkage. This is corroborated by the results reported here; as shown in Fig. 7, the mutation changes the hydrogen bonding pattern of the counterion complex such that bonding to the Schiff proton of water molecules becomes very weak. In the case of bR_{568} the mutant does not show such a large effect either in the observations or in the simulations. These results further support the suggestion that the Schiff base hydrogen in bR_{568} and bR_{548} is not hydrogen bonded directly to Asp-85 or Asp-212 but, rather, through water molecules.

Photocycle of bR_{548}

The key finding of our simulations is that the photocycle of bR_{548} leads to an L_{610} intermediate for which the Schiff base proton points towards the cytoplasmic side and loses contact with Asp-85, the normal proton acceptor. An intact hydrogen bonding network between the Schiff base proton and Asp-85 has been found for the simulated L_{550} intermediate of the bR_{568} photocycle, which allows proton transfer from the Schiff base to Asp-85 (unpublished results). However, our simulations suggest that such a network does not exist for the L_{610} intermediate after photoisomerization of bR_{548}. This could explain why the photocycle of bR_{548} lacks an M intermediate.

The simulations of the isomerization process also shed light on the question of how the photocycle of bR_{548} leaks into the photocycle of bR_{568}, which requires a rotation around the C_{15}-N bond. It is observed that, after light absorption, ~10% of the isomerized bR_{548} experiences an isomerization around two bonds producing the all-*trans*,15-*syn* isomer. The question arises as to how this conversion is realized. Some ex-

perimental data indicate that conversion from the bR_{548} to bR_{568} photocycle occurs early in the excited state (Korenstein and Hess, 1977; Varo and Bryl, 1988; Balashov et al., 1988; Gergely et al., 1994). Our simulations support the notion that the branching pathway is a 13-*cis*,15-*syn* → all-*trans*,15-*anti* isomerization during the initial photoreaction of bR_{548}. A possibility of a similar photoisomerization around two double bonds induced by a single photon absorption had been suggested earlier (Warshel, 1976) and has recently been demonstrated experimentally in visual pigment isomerization (Zhu and Liu, 1993).

We like to stress that the present theoretical treatment of bR is mainly lacking the quantitative quantum chemical description of the ground and excited state potential surfaces of retinal. We consider simulations that combine the required quantum chemical calculations with a molecular dynamics description as the most important issue for future study. These types of calculations would dramatically improve all facets of the modeling presented in this paper. It is believed (Balashov et al., 1993) that the dark adaptation process in bR occurs via corotation around the C_{13}-C_{14} and the C_{15}-N bonds and is catalyzed via protonation of the Asp-85 residue. Only rigorous quantum chemical calculations in which charges of various protein groups are explicitly included in the electronic Hamiltonian of retinal can be expected to describe reasonably well such phenomena. The same holds for modeling the photoisomerization process, in which case the charged side groups near retinal are expected to govern excited state processes (Kobayashi et al., 1990; Song et al., 1993). Obviously, one wishes to predict quantitatively the spectra of in situ retinal for bR_{568}, bR_{548}, mutants, and photocycle intermediates. By combining molecular dynamics and semi-empirical quantum techniques, some attempts have already been made to describe spectra and photodynamics of in situ retinal (Warshel et al., 1991). The ultimate goal, however, is a combination of ab initio quantum chemistry and molecular dynamics to reproduce consistently and quantitatively observed spectra, spectral widths, and dielectric relaxation times. Quantitative agreement between calculated and observed electronic spectra could provide a convenient means to prove the validity of models for the intermediates in bR photocycles.

REFERENCES

Albeck, A., N. Livnah, H. Gottlieb, and M. Sheves. 1992. C_{13} NMR-studies of model compounds for bacteriorhodopsin: facts affecting the retinal chromophore chemical-shifts and absorption maximum. *J. Am. Chem. Soc.* 114:2400–2411.

Aton, B., A. G. Doukas, D. Narva, R. Callender, and U. Dinur. 1980. Resonance Raman studies of the primary photo-chemical event in visual pigments. *Biophys. J.* 29:79–84.

Baasov, T., N. Friedmann, and M. Sheves. 1987. Factors affecting the C=N stretching in protonated retinal Schiff-base: a model study for bacteriorhodopsin and visual pigments. *Biochemistry.* 26:3210–3217.

Balashov, S. P., R. Govindjee, M. Kono, E. Imasheva, E. Lukashev, T. G. Ebrey, R. K. Crouch, D. R. Menick, and Y. Feng. 1993. Effect of the arginine-82 to alanine mutation in bacteriorhodopsin on dark adaptation, proton release, and the photochemical cycle. *Biochemistry.* 32:10331–10343.

Balashov, S. P., N. V. Karneyeva, F. F. Litvin, and T. G. Ebrey. 1991. Bathoproducts and conformers of all-*trans*- and 13-*cis*-bacteriorhodopsin at 90 K. *Photochem. Photobiol.* 54:949–953.

Balashov, S. P., F. F. Litvin, and V. A. Sineshchekov. 1988. Photochemical processes of light energy transformation in bacteriorhodopsin. *Sov. Sci. Rev. D. Physiochem. Biol.* 8:1–61.

Bashford, D., and K. Gerwert. 1992. Electrostatic calculations of the pK values of ionizable groups in bacteriorhodopsin. *J. Mol. Biol.* 224: 473–486.

Berendsen, H. J. C., J. P. M. Postma, W. F. van Gunsteren, A. DiNola, and J. R. Haak. 1984. Coupling to a heat bath. *J. Chem. Phys.* 81:3684–3688.

Birge, R. R. 1990. Photophysics and molecular electronic applications of the rhodopsins. *Annu. Rev. Phys. Chem.* 41:683–733.

Brooks, B. R., R. E. Bruccoleri, B. D. Olafson, D. J. States, S. Swaminathan, and M. Karplus. 1983. CHARMm: a program for macromolecular energy, minimization, and dynamics calculations. *J. Comp. Chem.* 4(2):187–217.

Brünger, A. T. 1988. X-PLOR: a system for x-ray crystallography and NMR. The Howard Hughes Medical Institute and Department of Molecular Biophysics and Biochemistry, Yale University, New Haven, CT.

Brünger, A. T. 1991. Simulated annealing in crystallography. *Annu. Rev. Phys. Chem.* 42:197–223.

Bryl, K., M. Taiji, M. Yoshizava, and T. Kobayashi. 1992. Light adaptation of dark-adapted bacteriorhodopsin studied by nanosecond time-resolved absorption spectroscopy. *Photochem. Photobiol.* 56:1013–1018.

Drachev, L. A., S. V. Dracheva, and A. D. Kaulen. 1993. pH dependence of the formation of an M-type intermediate in the photocycle of 13-*cis*-bacteriorhodopsin. *FEBS Lett.* 332:67–70.

Engelhard, M., B. Hess, G. Metz, W. Kreutz, F. Siebert, J. Soppa, and D. Oesterhelt. 1990. High resolution ^{13}C-solid state NMR of bacteriorhodopsin: assignment of specific aspartic acids and structural implications of single site mutations. *Eur. Biophys. J.* 18:17–24.

Gergely, C., C. Ganea, and G. Varo. 1994. Combined optical and photoelectric study of the photocycle of 13-*cis* bacteriorhodopsin. *Biophys. J.* 67:855–861.

Gerwert, K., B. Hess, J. Soppa, and D. Oesterhelt. 1989. Role of Asp-96 in proton translocation by bacteriorhodopsin. *Proc. Natl. Acad. Sci. USA.* 86:4943–4947.

Harbison, G., O. Smith, J. Pardoen, C. Winkel, J. Lugtenburg, J. Herzfeld, R. Mathies, and R. Griffin. 1984. Dark-adapted bacteriorhodopsin contains 13-*cis*,15-*syn* and all-*trans*,15-*anti* retinal Schiff bases. *Proc. Natl. Acad. Sci. USA.* 81:1706–1709.

Henderson, R., J. M. Baldwin, T. A. Ceska, F. Zemlin, E. Beckmann, and K. H. Downing. 1990. Model for the structure of bacteriorhodopsin based on high-resolution electron cryo-microscopy. *J. Mol. Biol.* 213: 899–929.

Hofrichter, J., E. R. Henry, and R. H. Lozier. 1989. Photocycle of bacteriorhodopsin in light- and dark-adapted purple membrane studied by time-resolved absorption spectroscopy. *Biophys. J.* 56:693–706.

Humphrey, W., I. Logunov, K. Schulten, and M. Sheves. 1994. Molecular dynamics study of bacteriorhodopsin and artificial pigments. *Biochemistry.* 33:3668–3678.

Iwasa, T., F. Tokunaga, and T. Yoshizawa. 1981. Photochemical reaction of 13-*cis*-bacteriorhodopsin studied by low temperature spectrophotometry. *Photochem. Photobiol.* 33:539–545.

Kakitani, T., H. Kakitani, H., Rodman, B. Honig, and R. Callender. 1983. Correlation of vibrational frequencies with absorption maxima in polyenes, rhodopsin, bacteriorhodopsin, and retinal analogs. *J. Phys. Chem.* 87:3620–3628.

Kalisky, O., C. R. Goldschmidt, and M. Ottolenghi. 1977. On the photocycle and light adaptation of dark-adapted bacteriorhodopsin. *Biophys. J.* 19: 185–189.

Khorana, H. G. 1988. Bacteriorhodopsin, a membrane protein that uses light to translocate protons. *J. Biol. Chem.* 263:7439–7442.

Kobayashi, T., M. Terauchi, T. Kouyama, M. Yoshizawa, and M. Taiji. 1990. Femtosecond spectroscopy of acidified and neutral bacteriorhodopsin. *SPIE J.* 1403:407–416.

Korenstein, R., and B. Hess. 1977. Hydration effects on *cis-trans* isomerization of bacteriorhodopsin. *FEBS Lett.* 82:7–11.

Kraulis, P. 1991. MOLSCRIPT: a program to produce both detailed and schematic plots of protein structures. *J. Appl. Cryst.* 24:946–950.

Lanyi, J. K. 1992. Proton-transfer and energy coupling in the bacteriorhodopsin photocycle. *J. Bioenerg. Biomembr.* 24:169–179.

Livnah, N. and M. Sheves. 1993. Model compounds can mimic spectroscopic properties of bovine rhodopsin. *J. Am. Chem. Soc.* 115:351.

Mathies, R. A., S. W. Lin, J. B. Ames, and W. T. Pollard. 1991. From femtoseconds to biology: mechanism of bacteriorhodopsin's light-driven proton pump. *Annu. Rev. Biochem. Bioeng.* 20:491–518.

Mukohata, Y., K. Ihara, K. Y. M. Uegaki, and Y. Sugiyama. 1991. Australian *Halobacteria* and their retinal-protein ion pumps. *J. Photochem. Photobiol.* 54:1039–1045.

Noguchi, T., S. Kolaczkowski, W. Gärtner, and G. H. Atkinson. 1990. Resonance raman spectra of 13-demethylretinal bacteriorhodopsin and of a picosecond bathochromic photocycle intermediate. *J. Phys. Chem.* 94: 4920–4926.

Nonella, M., A. Windemuth, and K. Schulten. 1991. Structure of bacteriorhodopsin and in situ isomerization of retinal: a molecular dynamics study. *J. Photochem. Photobiol.* 54(6):937–948.

Oesterhelt, D., J. Tittor, and E. Bamberg. 1992. A unifying concept for ion translocation in retinal proteins. *J. Bioenerg. Biomembr.* 24:181–191.

Ohno, K., Y. Takeuchi, and M. Yoshida. 1977. Effect of light-adaptation on the photoreaction of bacteriorhodopsin from *Halobacterium halobium*. *Biochim. Biophys. Acta.* 462:575–582.

Orlandi, G., and K. Schulten. 1979. Coupling of stereochemistry and proton donor-acceptor properties of a Schiff base: a model of a light-driven proton pump. *Chem. Phys. Lett.* 64:370–374.

Ottolenghi, M., and M. Sheves. 1989. Synthetic retinals as probes for the binding site and photoreactions in rhodopsins. *J. Membr. Biol.* 112: 193–212.

Rath, P., T. Marti, S. Sonar, H. G. Khorana, and K. J. Rothschild. 1993. Hydrogen bonding interactions with the Schiff base of bacteriorhodopsin. *J. Biol. Chem.* 268:17742–17749.

Roepe, P. D., P. L. Ahl, J. Herzfeld, J. Lugtenburg, and K. J. Rothschild. 1988. Tyrosine protonation changes in bacteriorhodopsin. *J. Biol. Chem.* 263:5110–5117.

Santarsiero, B. D., and M. N. G. James. 1990. Crystal structure of *N*-methyl-*N*-phenylretinal iminium perchlorate: a structural model for the bacteriorhodopsin chromophore. *J. Am. Chem. Soc.* 112:9416–9418.

Sawatzki, J., R. Fischer, H. Scheer, and F. Siebert. 1990. Fourier-transform raman spectroscopy applied to photobiological systems. *Biophysics.* 87: 5903–5906.

Schulten, K., and P. Tavan. 1978. A mechanism for the light-driven proton pump of *Halobacterium halobium*. *Nature.* 272:85–86.

Sheves, M., and T. Baasov. 1984. Factors affecting the rate of thermal isomerization of 13-*cis*-bacteriorhodopsin to all-*trans*. *J. Am. Chem. Soc.* 106:6840–6841.

Sheves, M., T. Baasov, N. Friedman, M. Ottolenghi, R. Feinmann-Weinberg, V. Rosenbach, and B. Ehrenberg. 1984. On the binding-site of bacteriorhodopsin: a study with artificial pigments. *J. Am. Chem. Soc.* 106:2435–2437.

Smith, S. O., H. J. M. de Groot, R. Gebhard, J. M. L. Courtin, J. Lugtenburg, J. Herzfeld, and R. G. Griffin. 1989. Structure and protein environment of the retinal chromophore in light- and dark-adapted bacteriorhodopsin studied by solid-state NMR. *Biochemistry.* 28:8897–8904.

Smith, S., A. Myers, J. Pardoen, C. Winkel, P. Mulder, J. Lugtenburg, and R. Mathies. 1984. Determination of retinal Schiff base configuration in bacteriorhodopsin. *Biophysics.* 81:2055–2059.

Smith, S. O., J. A. Pardoen, J. Lugtenburg, and R. A. Mathies. 1987. Vibrational analysis of the 13-*cis*-retinal chromophore in dark-adapted bacteriorhodopsin. *J. Phys. Chem.* 91:804–819.

Song, L., M. A. El-Sayed, and J. K. Lanyi. 1993. Protein catalysis of the retinal subpicosecond photoisomerization in the primary process of bacteriorhodopsin photosynthesis. *Science.* 261:891–894.

Sperling, W., P. Carl, C. N. Rafferty, and N. A. Dencher. 1977. Photochemistry and dark equilibrium of retinal isomers and bacteriorhodopsin isomers. *Biophys. Struct. Mechanism.* 3:79–94.

Sperling, W., C. Rafferty, K. Kohl, and N. Dencher. 1979. Isomeric composition of bacteriorhodopsin under different environmental light conditions. *FEBS Lett.* 97:129–132.

Steinberg, G., N. Friedman, M. Sheves, and M. Ottolenghi. 1991. Isomer composition and spectra of the dark and light adapted forms of artificial bacteriorhodopsins. *Photochem. Photobiol.* 54:969–676.

van Laarhoven, P. J. M., and E. H. L. Aarts. 1987. *Simulated Annealing: Theory and Application.* D. Reidel, Dordrecht, The Netherlands.

Varo, G., and K. Bryl. 1988. Light- and dark-adaptation of bacteriorhodopsin measured by a photoelectric method. *Biochim. Biophys. Acta.* 934:247–252.

Warshel, A. 1976. Bicycle-pedal model for the first step in the vision process. *Nature.* 260:679–683.

Warshel, A., Z. T. Chu, and J.-K. Hwang. 1991. The dynamics of the primary event in rhodopsins revisited. *Chem. Phys.* 158:303–314.

Zhou, F., A. Windemuth, and K. Schulten. 1993. Molecular dynamics study of the proton pump cycle of bacteriorhodopsin. *Biochemistry.* 32(9):2291–2306.

Zhu, Y., and R. Liu. 1993. Divergent pathways in photobleaching of 7,9-*dicis*-rhodopsin and 9,11-*dicis*-fluororhodopsin: one-photon-two-bond and one-photon-one-bond isomerization. *Biochemistry.* 32: 10233–10238.

Zinth, W., J. Dobler, M. A. Franz, and W. Kaiser. 1988. The primary steps of photosynthesis in bacteriorhodopsin. In *Spectroscopy of Biological Molecules: New Advances.* E. D. Schmid, F. W. Schneider, and F. Siebert, editors. Wiley, New York. 269–274.